PNAS RESEARCH ARTICLE | BIOPHYSICS AND COMPUTATIONAL BIOLOGY

Motorized chain models of the ideal chromosome

Zhiyu Cao[a,b] and Peter G. Wolynes[a,c,d,1]

Contributed by Peter G. Wolynes; received April 8, 2024; accepted June 6, 2024; reviewed by Masaki Sasai and Tongye Shen

An array of motor proteins consumes chemical energy in setting up the architectures of chromosomes. Here, we explore how the structure of ideal polymer chains is influenced by two classes of motors. The first class which we call "swimming motors" acts to propel the chromatin fiber through three-dimensional space. They represent a caricature of motors such as RNA polymerases. Previously, they have often been described by adding a persistent flow onto Brownian diffusion of the chain. The second class of motors, which we call "grappling motors" caricatures the loop extrusion processes in which segments of chromatin fibers some distance apart are brought together. We analyze these models using a self-consistent variational phonon approximation to a many-body Master equation incorporating motor activities. We show that whether the swimming motors lead to contraction or expansion depends on the susceptibility of the motors, that is, how their activity depends on the forces they must exert. Grappling motors in contrast to swimming motors lead to long-ranged correlations that resemble those first suggested for fractal globules and that are consistent with the effective interactions inferred by energy landscape analyses of Hi-C data on the interphase chromosome.

active matter | Hi-C | motor proteins | polymer physics | loop extrusion model

Significance

Motorized active processes enable changes of chromosome structure during the cell's life cycle. We put forward two families of motorized chain models and analyze how such motors influence the structure of idealized, homogeneous chromosomes. Swimming motors, akin to those found in the cellular cytoskeleton, act to globally extend and contract chains. In contrast, grappling motors, like those proposed in models of loop extrusion, induce long-ranged correlations that are consistent with the effective energy landscapes deduced by information-theoretic analyses of Hi-C contact maps on the interphase chromosome, which measure the frequency of crosslinking between all pairs of genomic loci.

Chromatin is intricately folded and regulated by a multitude of proteins (1–6). Both during mitosis and in interphase, the chromosome fluctuates and appears to be only partially structured (7–12). Hi-C experiments give us information about the chromosome's structural correlations by determining the contact probabilities between genomic loci pairs (7). The information from these experiments can be harvested using effective energy landscapes that assume the chromosome fiber interacts with itself via a potential energy at an effective temperature to give a Boltzmann distribution (13–19). This approach, while powerful, is agnostic concerning the detailed mechanism of structure formation. We recognize however that the cell nucleus is an active environment (16). Adenosine triphosphate (ATP)-driven molecular machines create specific structures and Brownian chain motion disorders them (20). Many chromatin-associated proteins are motors (21–23), such as RNA polymerases and the structural maintenance of chromosomes (SMC) complexes, all of which consume chemical energy (24) to perform nonequilibrium reactions and/or exert mechanical forces (25–28). Owing to these nonequilibrium mechanisms and the fact that the nucleus has history dependence in the cell cycle, there is no a priori guarantee that an effective equilibrium model rigorously applies. Nevertheless, it has been shown elsewhere, in models of the cytoskeleton, that motor activity can lead to statistics described by a quasi-equilibrium energy landscape when the active forces are not too large in comparison to the Brownian motion (29–32). A variety of models of chromosome structure formation are less agnostic and have already been proposed that use nonequilibrium motors (33–40). These models generally assume motors do not respond to forces.

Here, we will explore two classes of models, much richer than have so far been analyzed that do include such force response. We will explore an approximate statistical mechanical treatment of models of a motorized homogeneous chromosome. One class of motors we call "swimming motors." Swimming motors simply transit the polymer chain in three-dimensional space, but in contrast to earlier treatments of motorized chromosomes, may respond to the mechanical forces of the chains. We picture these swimming motors as providing crude caricatures of the effects of polymerases and other factors moving along the chains. We presently ignore the topological effects of such motors, such as supercoiling. We show such motors can act to expand or contract the chain depending on their susceptibility, but would leave it Rouse-like if they were the only actors. The second class of motors we call "grappling motors." These models caricature the loop extrusion process (41–45). We will show that in contrast to swimming motors, grappling motors induce effective long-ranged interactions between chain segments that give an effective energy landscape consistent with the ideal chromosome model that emerges

Author affiliations: [a]Center for Theoretical Biological Physics, Rice University, Houston, TX 77005; [b]Department of Chemical Physics, University of Science and Technology of China, Hefei, Anhui 230026, China; [c]Department of Chemistry, Rice University, Houston, TX 77005; and [d]Department of Physics, Rice University, Houston, TX 77005

Author contributions: Z.C. and P.G.W. designed research; performed research; analyzed data; and wrote the paper.

Reviewers: M.S., Kyoto Daigaku; and T.S., University of Tennessee at Knoxville.

The authors declare no competing interest.

[1]To whom correspondence may be addressed. Email: pwolynes@rice.edu.

This article contains supporting information online at https://www.pnas.org/lookup/suppl/doi:10.1073/pnas.2407077121/-/DCSupplemental.

Published July 2, 2024.

from the Hi-C data (13–18). To obtain these results, we show that an approximate variational treatment of the Master equation for motorized chain dynamics yields a self-consistent equation for these long-ranged interactions and using this treatment show that grappling motors can give rise to many generic but also detailed features observed in contact frequency maps, including the apparent fractal behavior of the long-ranged contact distribution.

Model and Theoretical Background

We will study a very simple case, an active homogeneous chromosome described as a Rouse homopolymer chain, which is acted upon by stochastic motorization. We can think of the motion as being described by an overdamped Langevin equation $\dot{\mathbf{r}}_i = \beta D(-\nabla_i U) + \boldsymbol{\eta}_i + \mathbf{v}_i^m$, but with the crucial addition of jumps due to the motors. Here, $\mathbf{r}_i$ is the position of the i-th bead, and the potential is harmonic, $U(\{\mathbf{r}\}) = U(\mathbf{r}_1, \mathbf{r}_2, \ldots, \mathbf{r}_n) = K\sum_{i=1}^{N}(\mathbf{r}_i - \mathbf{r}_{i-1})^2/2$ with K the spring constant. The random variable η encodes the ordinary thermal Brownian random forces that vanish on average. Their distribution is taken to be Gaussian, where $\langle \eta_{i_1}^{j_1}(t)\eta_{i_2}^{j_2}(t')\rangle = 2D\delta_{i_1 i_2}\delta_{j_1 j_2}\delta(t-t')$ with D the diffusion coefficient and β the inverse temperature. The motorized jump term $\mathbf{v}_i^m = \sum_q \mathbf{l}_q \delta(t-t_q)$ is a time series of shot-noise-like kicks. The nature of these discrete kicks depends on the way a motor responds to applied forces and on how the motor displaces chain elements. The stochastic nature of the motors is best captured by a Master equation for the dynamics of the probability distribution function Ψ of the chain having positions in three-dimensional space $\{\mathbf{r}_i\}$, $\partial_t \Psi_t(\{\mathbf{r}\}) = (\mathcal{L}_{FP} + \mathcal{L}_{NE})\Psi_t(\{\mathbf{r}\})$. The first part of the time development comes from $\mathcal{L}_{FP}\Psi_t(\{\mathbf{r}\}) = -\sum_i \nabla_i \cdot \mathbf{J}_i$, which is the conventional Fokker–Planck operator describing the passive Brownian dynamics in a field of conservative forces, where $\mathbf{J}_i(\{\mathbf{r}\};t) = \beta D(-\nabla_i U)\Psi_t(\{\mathbf{r}\}) - D\nabla_i \Psi_t(\{\mathbf{r}\})$ is the probability current. The other nonequilibrium term describes the motorized displacements of the chain by the motors which are regarded as making discrete jumps. We write for this contribution to the Master equation

$$\mathcal{L}_{NE}\Psi_t(\mathbf{r}) = \int \Pi_i d\mathbf{r}_i' K_{\mathbf{r}'\to\mathbf{r}}\Psi_t(\mathbf{r}') - \Psi_t(\mathbf{r})\int \Pi_i d\mathbf{r}_i' K_{\mathbf{r}\to\mathbf{r}'}. \quad [1]$$

Here, $K_{\mathbf{r}'\to\mathbf{r}}$ is the transition probability between different chromosome configurations caused by a single motor stepping event. The motor kicking rate $\kappa W(\Delta U)$ encodes the way in which the underlying biochemical mechanisms of the motors respond to the external forces needed to make the displacement. We write $W(\Delta U) = \Theta(\Delta U)e^{-\vartheta_u \beta \Delta U} + \Theta(-\Delta U)e^{-\vartheta_d \beta \Delta U}$ (29–32, 46, 47), κ the basal kicking rate, Θ the Heaviside function, and ΔU the free energy difference between the starting configuration and the displaced chain due to the motorization. We call the parameter ϑ the susceptibility of the motor. This quantity indicates the mechanical coupling between the motorized conformational remodeling and the local mechanical forces acting on the motor. Information about the susceptibility of biological motors has been obtained for many systems using force extension measurements (48, 49). Depending on the motor mechanism, one may have different values of the susceptibility for uphill kicks (ϑ_u) and for downhill kicks (ϑ_d). When $\vartheta = 0$, the motor does not respond to forces. We call it then a fully adamant motor. When $\vartheta \neq 0$, the motor responds to applied forces. Motors with both signs of ϑ are known. We here mainly focus on motors with nonnegative ϑ. Motors with negative ϑ so-called load-resisting motors also exist (50, 51). For simplicity in this paper, we take $\vartheta_u = \vartheta_d = \vartheta$ but our results are easily generalized.

Type of Motors. In the study of active matter, motors are often taken to displace their cargo directly in three-dimensional space. Strictly speaking, true swimming at the molecular level makes only small steps (52). We call such motors that displace elements individually "swimming motors." In a renormalized sense (51, 53), one imagines such a motor could roughly describe the local restructuring of chromatin by active nuclear enzymes such as RNA polymerase II, helicase, or topoisomerase (~5nm to 15nm in the kicking distance) (20, 54). In contrast to swimming (which acts on individual segments), extrusion requires two subunits to move with respect to each other. We call such two particle motions "grappling" motions. SMC complexes such as bacterial SMC, cohesin, and condensin (~50 nm in grappling distance) to first order can be thought of as "grappling motors" (55, 56).

Swimming motors. A swimming motor makes a power stroke which induces a discrete conformational change that ultimately moves the polymer bead by a distance l in a direction $\mathbf{n}$, i.e., $\mathbf{l} = l\mathbf{n}(\boldsymbol{r})$; see Fig.1. The integral kernel $K_{\mathbf{r}'\to\mathbf{r}}$ for a swimming motor can be written as

$$\mathcal{L}_{NE}\Psi_t(\mathbf{r}) = \kappa\sum_i \int d\mathbf{n} \{e^{-\vartheta\beta[U(\ldots,\mathbf{r}_i,\ldots)-U(\ldots,\mathbf{r}_i-\mathbf{l},\ldots)]}\Psi_t(\ldots,\mathbf{r}_i'=\mathbf{r}_i-\mathbf{l},\ldots) - e^{-\vartheta\beta[U(\ldots,\mathbf{r}_i+\mathbf{l},\ldots)-U(\ldots,\mathbf{r}_i,\ldots)]}\Psi_t(\ldots,\mathbf{r}_i,\ldots)\}. \quad [2]$$

The motor kicking rate may be sequence-dependent or configuration-dependent (52). Here, we will assume that the kicking direction $\mathbf{n}$ fluctuates on a timescale $\tau \ll \kappa^{-1}$ of the motor particle tumbling, which corresponds to an isotropic kicking process. For instance, polymerases, etc, swim along the chain but local motions of the chain should ultimately lead to isotropy. In our coarse-grained model, the persistence length is small, so isotropy is a good first approximation.

Grappling motors. Our caricature of a grappling motor is based on the "swing and clamp" model proposed for the loop extrusion process (42). Quite similar motions, different in detail, have also been referred to as the "reel and seal" model (44) and "heed and feed" model (45). At the Master equation level, these are

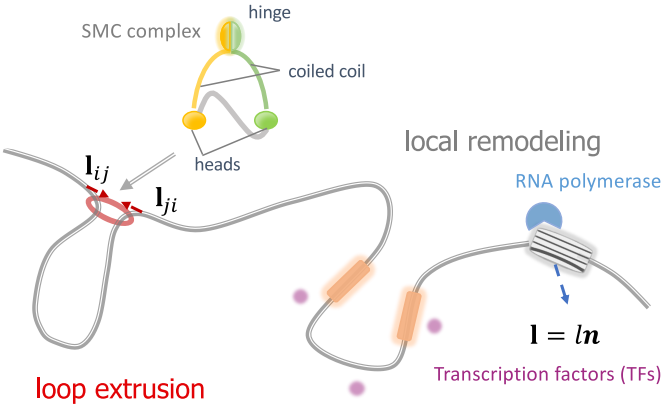

Fig. 1. Chromosome dynamics involves several motorized processes. Many motors act locally to allow the chain to swim. The SMC complex actively extrudes loops by interacting with DNA segments through ATP consumption. It involves a grappling process in which segments some distance away from each other can be brought together.

essentially equivalent. In these models, part of a DNA loop is first clamped near the ATPase head of the motor, while the hinge domain at the other end extends to grasp some surrounding DNA segment if it is available. Subsequently, the coil bends, "swinging" the hinge with the new DNA segment close to the head, where it becomes sealed onto the head and merges with the DNA loop. The long coiled-coil of the SMC complex is not merely an inert linker between the head and the hinge domains of SMC, but a critical participant in loop extrusion in this view (57–62). The twisting and writhing of the coiled-coil, coupled with the movement of the SMC head domain, would allow such motors to remodel the topological structure of DNA. Krepel et al. suggested such a mechanism through a simulation study based on an energy landscape optimized force field (AWSEM) along with coevolutionary information. Their model suggested the chains could braid and thus explained some otherwise puzzling crosslinking data on the cohesin molecule in vivo (63). Our present model does not explicitly deal with these topological effects, which could directly propagate along the chromosome fibers.

Based on the above description, the loop extrusion effect is generated by anticorrelated grappling on pairs of nodes (i,j) on the chain, where one side corresponds to the anchor point that is bound to the head, while the other side represents the segment eventually grasped by the hinge. A clamped kick is thus represented by a pair of displacements along the line of centers $(\mathbf{l}_{ij},\mathbf{l}_{ji}) = l(\hat{\mathbf{r}}_{ij},-\hat{\mathbf{r}}_{ij})$, where l is the kick size which should be roughly the size of the SMC motor and $\hat{\mathbf{r}}_{ij}$ is a unit vector pointing from node i to node j; see Fig.1. The effective rates κ, kicking distance l, and diffusion constant D are typically different in magnitude for the swimming motors and grappling motors—l being much larger for cohesins, etc, than polymerases. By omitting other particles' positions except those involved in the kicks in the expression of free energy and configuration, the dynamical evolution of the many-particle configuration due to these motor-driven processes can be expressed by a sum of two-particle stochastic displacement operators,

$$\begin{aligned}&\mathcal{L}_{NE}\Psi_t(\mathbf{r})\\&=\frac{1}{2}\kappa\sum_i\sum_j\int d\mathbf{r}_i'\int d\mathbf{r}_j'\{\mathcal{C}(r_{ij}')\delta(\mathbf{r}_i-\mathbf{r}_i'-\mathbf{l}_{ij})\\&\times\delta(\mathbf{r}_j-\mathbf{r}_j'+\mathbf{l}_{ij})e^{-\vartheta\beta[U(\mathbf{r}_i,\mathbf{r}_j)-U(\mathbf{r}_i',\mathbf{r}_j')]}\Psi_t(\mathbf{r}_i')-\mathcal{C}(r_{ij})\\&\times\delta(\mathbf{r}_i-\mathbf{r}_i'+\mathbf{l}_{ij})\delta(\mathbf{r}_j-\mathbf{r}_j'-\mathbf{l}_{ij})e^{-\vartheta\beta[U(\mathbf{r}_i',\mathbf{r}_j')-U(\mathbf{r}_i,\mathbf{r}_j)]}\Psi_t(\mathbf{r}_i)\}.\end{aligned}\quad[3]$$

Here, κ is a basal composite grappling rate, while the rate of potential grappling events also will depend on the instantaneous chromosome conformation and the motor susceptibility. The grappling probability $\mathcal{C}(r_{ij})$ describes the tendency of having a loop grappling event involving the i-th and j-th beads, which is a function $r_{ij}=|\mathbf{r}_i-\mathbf{r}_j|$.

Péclet Number Expansion. Wang and Wolynes showed that when the kicking lengths are small, one can expand the probability distribution function in powers of l up to the quadratic order to obtain a system that is described still by a many-body diffusion equation but with modified forces and modified diffusion constants (31, 32, 64). They applied this expansion to study the self-organization and aging behaviors of the active cytoskeleton and the dynamic remodeling of actomyosin networks.

Expansion for swimming motors. For swimming motors, the nonequilibrium kicking operator to quadratic order in l has a quasi-equilibrium form (*SI Appendix*)

$$\mathcal{L}_{NE}\Psi_t(\mathbf{r})=-\sum_i\nabla_i\cdot\left[\frac{\vartheta\kappa l^2}{d}(-\nabla_i\beta U)\Psi_t(\mathbf{r})-\frac{\kappa l^2}{2d}\nabla_i\Psi_t(\mathbf{r})\right].\quad[4]$$

We see the effect of the motor is to obtain an effective diffusion constant for the Brownian motion and an effective temperature renormalizing the effect of the actual forces,

$$\frac{D_{\text{eff}}}{D}=1+\frac{\kappa l^2}{2dD},\quad\frac{\beta_{\text{eff}}}{\beta}=1+\left(\vartheta-\frac{1}{2}\right)\frac{\kappa l^2}{dD}.\quad[5]$$

Here, d is the general dimension. We call the quantity $\kappa l^2/D$ the Péclet number, in analogy to problems involving diffusion along with convection hydrodynamics. The Péclet number measures the effects of flows relative to thermal diffusions. Swimming motors generally enhance diffusion and lead to an effective temperature which may be bigger or smaller than the ordinary temperature depending on the motor susceptibility.

Expansion for grappling motors. For grappling motors, an effective kicking diffusional operator can also be obtained by similar mathematical manipulations now for the pair displacement operator (32, 47, 50). The effective dynamical equation again to quadratic order reads (*SI Appendix*)

$$\begin{aligned}\mathcal{L}_{NE}\Psi_t(\mathbf{r})=\sum_i\Bigg[&\frac{1}{2}\kappa l^2\sum_{j\neq i}\hat{\mathbf{r}}_{ij}\hat{\mathbf{r}}_{ij}:\nabla_i\nabla_i\mathcal{C}_{ij}\Psi+\beta\vartheta\kappa l^2\\&\times\left(\sum_{j\neq i}\hat{\mathbf{r}}_{ij}\hat{\mathbf{r}}_{ij}:(\nabla_i\mathcal{C}_{ij}\Psi\nabla_i\beta U+\mathcal{C}_{ij}\Psi\nabla_i\nabla_i U)\right]\\&-\sum_i\sum_{j\neq i}\Bigg[\frac{1}{2}\kappa l^2\hat{\mathbf{r}}_{ij}\hat{\mathbf{r}}_{ij}:\nabla_i\nabla_j\mathcal{C}_{ij}\Psi\\&+\beta\vartheta\kappa l^2\hat{\mathbf{r}}_{ij}\hat{\mathbf{r}}_{ij}:(\nabla_i\mathcal{C}_{ij}\Psi\nabla_j\beta U+\mathcal{C}_{ij}\Psi\nabla_i\nabla_j U)\Bigg],\end{aligned}\quad[6]$$

where $\mathcal{C}_{ij}=\mathcal{C}(r_{ij})$. We see now that in contrast to swimming motors, the effective diffusion constant and the effective temperature depend on chain configuration

$$\mathbf{D}_{\text{eff},ii}=D\mathbf{I}+\frac{1}{2}\kappa l^2\sum_{j\neq i}\mathcal{C}_{ij}\hat{\mathbf{r}}_{ij}\hat{\mathbf{r}}_{ij},\quad\mathbf{D}_{\text{eff},ij}=-\frac{1}{2}\kappa l^2\mathcal{C}_{ij}\hat{\mathbf{r}}_{ij}\hat{\mathbf{r}}_{ij},\quad[7]$$

and

$$\boldsymbol{\beta}_{\text{eff},ii}=\beta\left[\mathbf{I}+\left(\vartheta-\frac{1}{2}\right)\frac{\kappa l^2}{D}\sum_{j\neq i}\mathcal{C}_{ij}\hat{\mathbf{r}}_{ij}\hat{\mathbf{r}}_{ij}\right],\quad\boldsymbol{\beta}_{\text{eff},ij}=2\vartheta\beta\boldsymbol{I}.\quad[8]$$

Here, $\boldsymbol{I}$ is the identity matrix in three-dimensional space. One also finds an additional potential coming from the grappling processes (*SI Appendix*),

$$U_{\text{mod}}(r_{ij})\approx U(r_{ij})+\mathcal{C}(r_{ij})\frac{\kappa l^2}{\beta D}\ln r_{ij}+\frac{\kappa l^2}{\beta D}g(r_{ij}),\quad[9]$$

where $g(r)=-\int dr\mathcal{C}'(r)/r$. For grappling motors, both $\boldsymbol{D}_{\text{eff}}$ and $\boldsymbol{\beta}_{\text{eff}}$ become configuration-dependent tensors, that depend on the distribution of extrusion probability. Again,

whether self-diffusion is enhanced, and how the local effective temperature is modified depends on the motor susceptibility, as for the swimming motor. We see however that the grappling motion specifically induces mutual diffusion and changes the effective temperatures relevant to the direct interactions between segments. These effects resemble the hydrodynamic interactions studied in polymer physics when we move to the Zimm model (65). Because the effective temperatures are also configuration-dependent, structural correlations become modified in contrast to what happens with hydrodynamic interactions. In Eq. **9**, the potential is also modified by two additional pairwise terms. The first term of this modification is induced by the grappling effect, providing an effective short-ranged attraction (32). The second term comes from the gradient of the grappling probability. Usually, two particles that are closer together have a higher tendency to be involved in a grappling event, so this term provides an additional attraction in general (64).

Effective Rouse Mode Analysis. If we ignore the excluded volume and average over the nonlinearity of the induced interactions, we can still use an effective Rouse model for the renormalized dynamics that come from the motors to quadratic order in l. It is easiest to see this in a continuous version of the model. Assuming a long polymer chain, composed of a large number of beads, the dynamics can be simplified to a continuous version $\mathbf{r}_i(t) \to \mathbf{r}(s,t)$ as $\partial_t \mathbf{r}(s,t) = (\beta D) K \partial_s^2 \mathbf{r}(s,t) + \boldsymbol{\eta}(s,t)$ (66, 67). Here, s represents a continuous chain sequence index along the polymer. The continuous model facilitates our analytical calculation of large loops, where the Rouse mode decomposition can be written as $\mathbf{r}(s,t) \to \hat{\mathbf{r}}_q(t) = \int_{-L/2}^{L/2} ds e^{-iqs} \mathbf{r}(s,t)$ and $\boldsymbol{\eta}(s,t) \to \hat{\boldsymbol{\eta}}_q(t) = \int_{-L/2}^{L/2} ds e^{-iqs} \boldsymbol{\eta}(s,t)$ with L the polymer length. The Rouse modes can be represented by the matrix $\hat{\mathbf{R}}(t)$ with $\hat{\mathbf{R}}_{q,\ldots}(t) = \hat{\mathbf{r}}_q(t)$. Then, one can capture the steady-state conformation of the polymer by calculating the second Rouse moments (38)

$$\mathbf{Y} = \lim_{t\to\infty} \langle \hat{\mathbf{R}}(t) \cdot \hat{\mathbf{R}}^{\dagger}(t) \rangle / L. \qquad [10]$$

For algebraic simplicity, we will also apply periodic boundary conditions to the entire chain effectively closing it into a circle. This avoids consideration of the end effects. By transforming Eq. **10** into real sequence space, we get the mean squared separation $\langle \mathbf{r}_{ss'}^2(t) \rangle$ with $\mathbf{r}_{ss'}(t) = \mathbf{r}(s,t) - \mathbf{r}(s',t)$, which describes the patterns in the polymer conformation. We assume the chain contour length is much longer than the genomic distance we focus on and therefore ignore specific end effects.

Swimming Motors Cause Uniform Local Chain Renormalization

When only swimming motors acting on each chain segment are involved, for the Rouse chain, as shown in *SI Appendix*, the separation between sequence locations s and s' subjected to swimming motors in the steady state is simply renormalized

$$\langle r_{ss'}^2 \rangle = b^2 |\Delta s| \left[1 - \left(\vartheta - \frac{1}{2} \right) \frac{\kappa l^2}{dD} \right], \qquad [11]$$

where $r_{ss'} = |\mathbf{r}_{ss'}|$ is the interparticle separation, $\Delta s = |s - s'|$ is the genomic distance and $b = \sqrt{3/\beta K}$ is the Kuhn length of polymer chain. More susceptible motors ($\vartheta > 1/2$), cause the polymer chain's local constraints to appear stronger, resulting in a contraction. As the motors become adamant ($\vartheta < 1/2$), the constraints appear weaker and the chain expands as expected for an increased effective temperature. For $\vartheta = 1/2$, the motors obey detailed balance so the original equilibrium would not be disturbed. We also have obtained these results by using the self-consistent phonon theory (68–71) accounting for nonlinearities (*SI Appendix*). This self-consistent approach was previously used for cytoskeletal models (29, 30, 46), and has been extended to network systems (72). More generally, for the case where the response to forces is asymmetric between uphill and downhill moves, the chain tends to contract when $\vartheta_u + \vartheta_d > 1$ and expand when $\vartheta_u + \vartheta_d < 1$.

The results for adamant swimming motors (that polymer segments locally expand compared to the passive counterpart) are consistent with previous studies of models with perfectly persistent active processes (34–36, 38–40). Such a motorized structure change seems consistent with the morphology of euchromatin and heterochromatin (73, 74). Euchromatin typically requires ATP consumption to maintain its expanded state, as has been experimentally observed by displacement correlation spectroscopy (20). The motor's active noise-generating persistent motion leads to a higher effective temperature. A completely adamant motor ($\vartheta = 0$) in the Master equation description can be directly mapped to the active Brownian particle model and the active Ornstein–Uhlenbeck model (75) (*SI Appendix*). On the other hand, it has sometimes been reported that activity can sometimes also lead to a denser packing of the chromatin fibers, akin to squeezing or compacting the chain (39, 76). We see that susceptible motors might be able to capture such local contraction phenomena while other rigid adamant motor models lead to chain expansion.

To further confirm our analytical prediction, we compare the numerical results of simulations of chains with such motors (*Bottom* triangle) and the analytical results from Eq. **11** (*Upper* triangle) for the mean-squared separation $\sqrt{r_{ss'}^2}$ in Fig. 2. The numerical data were obtained by performing a hybrid Brownian dynamics simulation for finite-length polymer chains with additional stochastic steps (*Materials and Methods*). We show the results both for the perfectly adamant motor ($\vartheta = 0$, *Left*

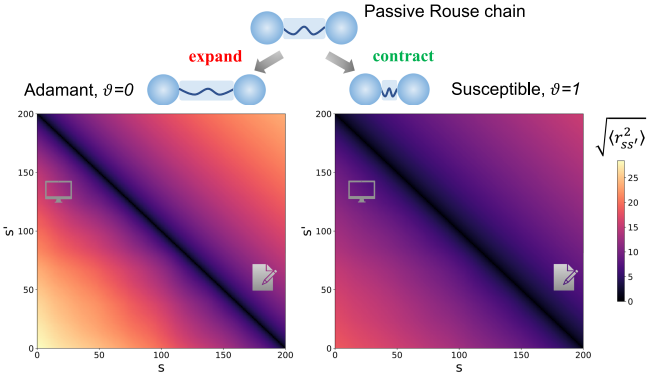

Fig. 2. The mean-squared separation $\sqrt{\langle r_{ss'}^2 \rangle}$ of motorized polymer chain for both the adamant swimming motor ($\vartheta = 0$, *Left* panel) and the susceptible swimming motor ($\vartheta = 1$, *Right* panel). The results obtained from Brownian dynamics simulations are presented in the *Bottom* triangle section of each panel, whereas the *Upper* triangle region shows the results from Eq. **11**. Parameters $\kappa l^2/dD = 1$ and $b^2 = 2$ for both panels. The adamant motor causes chain expansion, while the susceptible motors lead to chain contraction. Additionally, our simulation results demonstrate that the reorganization of motorized homopolymer chains is uniform.

panel) and the highly susceptible motor ($\vartheta = 1$, *Right* panel) for the case $\kappa l^2/dD = 1$ and $b^2 = 2$. The simulation results also demonstrate that the reorganization of homopolymer chains caused by swimming motors remains uniform in the absence of the grappling and the chain still has free-chain-like statistics. The simulation results for the effective Kuhn length are slightly higher than the theoretical predictions. This is an effect of the finite length of the polymer chains which are not cyclic in the simulations. The chain ends become more flexible due to not being dragged as much by the remainder of the chain, reducing the overall apparent rigidity of the chains.

Grappling Motors

The Self-Consistent Phonon Approximation. Since the grappling rate depends on the proximity of the chain segments that are moved, the Rouse model can only be an approximation. The chain is not strictly speaking harmonic. We must then make a mean field ansatz to determine the extrusion probabilities and the chromosome conformation statistics in a self-consistent manner. We assume the new Rouse modes have renormalized fluctuations but remain still approximately harmonic. We thus choose a trial Hamiltonian $\Psi(\hat{\mathbf{R}}) = \exp(-L^{-1}\sum_q \hat{\mathbf{r}}_q^2/Y_q^G)$ in the Fourier transformed coordinates with $Y_q^G = Y_{qq}^G$ to calculate the steady-state distribution by solving the Master equation with a variational approximation (77–80). This is very analogous to the self-consistent phonon approximation used for the cytoskeleton (29, 30, 46) but now we are treating the comparison system as a Debye model rather than an Einstein crystal. The argument found in *SI Appendix* yields:

$$Y_q^G \approx b^2\left[\frac{1}{q^2} - \frac{\kappa l^2}{dD}\frac{1}{q^4}\iint d\Delta s \frac{d^3k}{(2\pi)^3} b^2\langle \mathcal{C}(r_{\Delta s})\rangle \sin^2 \times \left(\frac{q\Delta s}{2}\right) e^{-k^2b^2|\Delta s|/4} - \left(\vartheta - \frac{1}{2}\right)\frac{\kappa l^2}{dD} \times \frac{\left(\int d\Delta s\langle \mathcal{C}(r_{\Delta s})\rangle + \int d\Delta s\langle \mathcal{C}(r_{\Delta s})\rangle e^{-iq\Delta s}\right)}{q^2}\right], \quad [12]$$

where $r_{\Delta s} = r_{ss'}$. In Eq. **12**, the second term will lead to a local renormalization of the effective short-range attraction, independent of susceptibility ϑ. The third term arises from the structure dependence of the correlation-induced grappling and is dependent on susceptibility ϑ. This long-range effect shows the configurational statistics is no longer simply free-chain-like. In the self-consistent mean-field assumption, the $r_{ss'}$ dependence of $\mathcal{C}(r_{ss'})$ leads to an averaged grappling probability $\tilde{\mathcal{C}}(s, s')$, so that the effective interactions, diffusion, and temperature all, on average, can then be expressed as scalar functions of genomic distance. $\tilde{\mathcal{C}}(s, s')$ is a probability density, which quantifies the probability of a grappling event occurring between two sites s and s'. For a uniform chain with sequence translational symmetry, one has $\tilde{\mathcal{C}}(s, s') = \mathscr{C}(\Delta s)$ and the (local) total grappling probability $\mathcal{C}_T = \int d\Delta s \mathscr{C}(\Delta s)$. The (local) total extrusion probability quantifies the (total) probability of a grappling event occurring between site s and other sites. We see in this approximation that when a pair of gene loci come into contact, the gain/loss of effective free energy from grappling only depends on the genomic distance between the segments when there is sequence translational invariance. Since grappling effects depend on genomic distance, there is a change in the structure of even a uniform chromosome.

Since grappling only occurs when two loci are within the range $[0, 2l)$, the averaged grappling probability between pairs of segments is proportional to the probability of the sites being within the grappling range $\mathrm{Prob}[r_{ss'} < 2l]$. Since the chain remains Gaussian, one finds $\tilde{\mathcal{C}}(s, s') = 2\mathcal{T}\mathrm{Prob}[r_{ss'} < 2l] \approx 2\mathcal{T}\sqrt{6/\pi}(2l)^3\langle r_{ss'}^2\rangle^{-3/2}$, where the second equality is obtained because within the self-consistent Rouse mode approximation the probability distribution remains Gaussian. Here, $\mathcal{T}$ is the average occupancy of cohesin, which is determined by the cohesin's affinity for the chains, its concentration, and its activity (81–83).

Grappling-Induced Local Renormalization. The contraction caused by the effective short-ranged grappling induced attraction turns out to be described by there being a smaller effective Kuhn length b_G (77–80, 84, 85) (*SI Appendix*),

$$Y_q^G = b^2\left[\frac{1}{q^2} - \frac{\kappa l^2}{dD}\frac{C_0}{q^2} - \left(\vartheta - \frac{1}{2}\right)\frac{\kappa l^2}{dD}\frac{(\mathcal{C}_T + \mathscr{C}_q)}{q^2}\right] \approx b_G^2\left[\frac{1}{q^2} - \left(\vartheta - \frac{1}{2}\right)\frac{\kappa l^2}{dD}\frac{(\mathcal{C}_T + \mathscr{C}_q)}{q^2}\right], \quad [13]$$

where $\mathscr{C}_q$ is the sequence Fourier transformation of the averaged extrusion probability $\mathscr{C}(\Delta s)$ and $C_0 \approx \sqrt{\pi}\mathscr{C}(0)(3 - 2\gamma_e - 2\log 2 - 2\log s_0)/8b$. γ_e is the Euler constant and s_0 is the minimum distance in sequence at which grappling can occur. The effective Kuhn length renormalization from this term $b_G/b = (1 - \frac{\kappa l^2}{dD}C_0)^{1/2} = 1 - o(l^2)$ is independent of motor susceptibility ϑ.

Long-Ranged Effect of Grappling Motors. The correlations induced by grappling motors depend on the chain's structure and are not localized in genomic distance. Within the self-consistent phonon approximation, one finds a generalized Rouse model that has weak long-ranged harmonic interactions. Again for grappling motors, we would find in addition to the usual local Rouse Hamiltonian a more distant coupling in the equation of motion:

$$\partial_t \mathbf{r}(s, t) = \beta D K_G\{\partial_s[(1 + \tilde{\mathcal{K}}(s))\partial_s \mathbf{r}(s, t)] + \int ds' \tilde{\mathcal{K}}_{LR}(s, s')[\mathbf{r}(s', t) - \mathbf{r}(s, t)]\} + \eta(s, t) \quad [14]$$

with $\beta K_G = 3/b_G^2$. The additional interactions caused by the grappling motors decouple into a local reorganization term $\tilde{\mathcal{K}}(s)$ and a direct interaction term $\tilde{\mathcal{K}}_{LR}(s, s')$ with reciprocity $\tilde{\mathcal{K}}_{LR}(s, s') = \tilde{\mathcal{K}}_{LR}(s', s)$. Under the sequence translational symmetry relevant to the circular chain, one finds through the variational approximation, a grappling-induced local renormalization and a grappling-induced long-ranged interaction (*SI Appendix*),

$$\tilde{\mathcal{K}}(s) = \left(\vartheta - \frac{1}{2}\right)\frac{\kappa l^2}{dD}\mathcal{C}_T, \quad [15]$$

$$\tilde{\mathcal{K}}^{LR}(s, s') = -\left(\vartheta - \frac{1}{2}\right)\frac{\kappa l^2}{dD}(\partial_s^2 + \partial_{s'}^2)\tilde{\mathcal{C}}(s, s'), \quad [16]$$

$\tilde{\mathcal{K}}(s)$ for the uniform chain renormalizes the effective Kuhn lengths, while the nonlocal $\tilde{\mathcal{K}}_{LR}(s, s')$ for a uniform chain gives rise to correlations like those of the "ideal chromosome" potential. The analysis can be extended to nonuniform situations (*SI Appendix*). The effective long-ranged interactions depend on

the mechanical properties of the motor through the susceptibility. The dependence of the Kuhn length renormalization on susceptibility aligns with what was observed for swimming motors. The long-ranged terms however also depend on the spatial distribution of the averaged extrusion probability, which in turn depends on the new structural correlation. Our results show that the effective temperature of the system with susceptible motors is lower than the thermal temperature. This may be related to the formation of liquid crystal structures of chromosomes under temperature quenching, as discovered in the information theoretic landscape studied by Zhang and Wolynes (13).

The Self-Consistent Equation for the Averaged Grappling Probability. Transforming Eq. **12** into real sequence space, one finds the mean squared separation between chain segments for the uniform chain becomes (*SI Appendix*)

$$\langle r_{ss'}^2\rangle = b_G^2|\Delta s|\left[1-\left(\vartheta-\frac{1}{2}\right)\frac{\kappa l^2}{dD}\mathcal{C}_T\right] + b_G^2\left(\vartheta-\frac{1}{2}\right)\frac{\kappa l^2}{dD}\int_0^{\Delta s} dx\mathscr{C}(x)(\Delta s-x). \quad [17]$$

In addition to the local renormalization of the Kuhn length caused by the grappling motors, we see there is a convolution of the averaged grappling probability $\tilde{\mathcal{C}}(s,s') = \mathscr{C}(\Delta s)$, which describes the effects of loop extrusion on long-ranged structural correlations.

We are thus led to a self-consistent equation for the averaged grappling probability $\mathscr{C}(\Delta s)$ in the steady states using the effective Kuhn length:

$$\frac{\mathscr{C}(\Delta s)}{B\mathcal{T}} = \left[|\Delta s|(1-\frac{Q\mathcal{C}_T}{\mathcal{T}}) + Q\int_0^{\Delta s}\frac{\mathscr{C}(x)}{\mathcal{T}}(\Delta s-x)dx\right]^{-\frac{3}{2}}. \quad [18]$$

Here, $B = 2\mathcal{T}\sqrt{6/\pi}(2l/b_G)^3$ is a dimensionless parameter, depending on the cohesin occupancy and the ratio of kick size to grappling renormalized effective Kuhn length b_G. Eq. **18** provides a closure that can be numerically solved, where the motor susceptibility ϑ, motor activity $\kappa l^2/dD$ and average cohesin occupancy $\mathcal{T}$ appear together in a simple composite form

$$Q = \left(\vartheta-\frac{1}{2}\right)\frac{\kappa\mathcal{T}l^2}{dD},$$

which we referred it as the nonequilibrium factor. For low cohesin occupancy ($\mathcal{T}\to 0$) or small motor activity ($\kappa l^2/D\to 0$), $Q = 0$. We see grappling will not change the structure if the motors obey detailed balance ($\vartheta = 1/2$). Since $\langle r_{ss'}^2\rangle \propto (\mathscr{C}/\mathcal{T})^{-2/3}$, it can be observed from Eq. **18** that the chromosome conformation depends only on the Q value. The self-consistent equation is pivotal in deciphering the loop extrusion effect.

Shapes of Contact Frequency

The Hi-C experiments, which generate contact frequency maps $P_c(s,s')$ between all pairs of genomic positions s and s', describe the characteristics of chromosome folding across scales (7). For uniform chains, the physical state of the chromosomes can be summarized by a power law scaling of the average contact frequency $P_c(s,s') = P_c(\Delta s)\propto \Delta s^{-\gamma}$ with genomic distance Δs, where γ is the scaling exponent (86). For fixed cutoff contact radius a_0, $P_c(\Delta s) = \mathrm{Prob}[r_{ss'}(t) < a_0] \approx \sqrt{6/\pi}a_0^3\langle r_{ss'}^2\rangle^{-3/2}$. Previous studies have shown that by this measure chromosome structures apparently possess fractal dimensions and are "crumpled" states, since the contact frequency shows a slower decay with Δs than the classical Rouse chain (7, 87–95). There is also evidence that the $P_c(\Delta s)$ curve does not always exhibit power-law behavior but may have, in addition, characteristic "shoulders," reflecting the folding of the chain into larger loops (95–97).

Numerical Results from the Self-Consistent Phonon Analysis. The power-law scaling of the averaged contact frequency is controlled by the power-law scaling of the averaged grappling probability. Since the self-consistent equation determines the extrusion probability, it provides a quantitative framework for understanding the typically observed shapes of contact frequency profiles.

In Fig. 3, we have numerically solved the self-consistent closure Eq. **18** to find several distinct contact frequency shapes depending on the nonequilibrium factor Q. The simulation and model details can be found in *Materials and Methods*. First, we focus on the effects of susceptible motors with $Q > 0$. For systems that are close to equilibrium with $Q\to 0$, the system still exhibits a classical Rouse-like scaling relationship $\Delta s^{-1.5}$. As the nonequilibrium factor Q increases to 0.13, the contact frequency profile begins to exhibit a nonuniform scaling behavior. At small scales, the system has a slower decay with Δs than the classical Rouse scaling. The scale of $P(\Delta s)\sim \Delta s^{-1.2}$ indicates that on these scales the polymer is in a crumpled state with fractal dimensions (95, 98, 99). At larger Δs scales, the

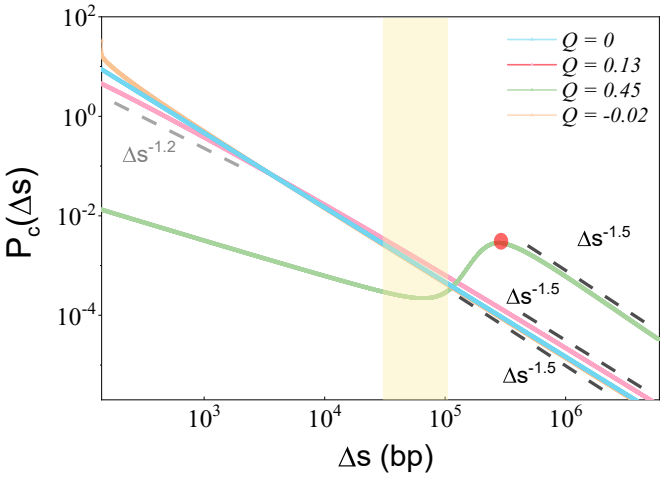

Fig. 3. Contact frequency plots as a function of the nonequilibrium factor $Q = (\vartheta-1/2)\kappa\mathcal{T}l^2/dD$. For $Q\to 0$, the system still exhibits largely Rouse-like scaling $\Delta s^{-1.5}$. When $Q = 0.13$, the contact frequency profile exhibits a nonuniform scaling behavior. At small scales, the system has a slower decaying than the classical Rouse scaling $P(\Delta s)\sim\Delta s^{-1.2}$, but the Rouse chain scaling $\Delta s^{-1.5}$ is restored at larger scales. The crossovers between different scaling behaviors occur in the yellow-shaded region. When $Q = 0.45$, the plot displays a nonmonotonic "shoulder," which suggests that segments of the polymer chain at distant locations appear to be involved in stable loops. The nonmonotonic "shoulder" in the contact frequency predicts the most probable loop size, indicated by the red dot. The decay of contact frequency beyond the loop size still follows the Rouse chain scaling $\Delta s^{-1.5}$. Finally, for the adamant case $Q = -0.02 < 0$, the segments exhibit larger contact probabilities at small scales while still recovering the Rouse scaling at larger scales. This phenomenon remains with further increasing $|Q|$ ($Q < 0$) until the numerical solution diverges at small scales for the chain without excluded volume.

Rouse chain scaling $\Delta s^{-1.5}$ is restored. The crumpled states have a smaller contact frequency for short genomic distances than the original Rouse chain but the contact frequency decays more slowly with genomic separation, finally exhibiting larger contact frequencies at larger scales than would the classical Rouse chains. The crossover between these behaviors occurs in the range of 10^4 to 10^5 bp. We see that the loop extrusion by grappling motors brings distant loci closer together. Finally, for very active grappling motors, as the Q value increases further to 0.45, the polymer chain begins to exhibit a nonmonotonic "shoulder." Apparently, segments of the polymer chain at distant locations come even closer together than expected due to the formation of fairly stable loops. The nonmonotonic "shoulder" in the contact frequency predicts the most probable loop size, which is approximately in the range of 10^5 to 10^6 bp (for realistic value of Q, see *SI Appendix*). Others have suggested that such a most probable size might prevent entanglements during the cell cycle (100–102). In our present analysis, the decay of the contact frequency outside the loop size returns to the Rouse chain scaling $\Delta s^{-1.5}$ as expected. For the more adamant case $Q = -0.02 < 0$, the segments have higher contact probabilities at small scales but then recover the Rouse scaling at larger genomic separation. We find however further increasing the magnitude of Q for Q negative leads to divergent numerical solutions at small scales, suggesting collapse that cannot be avoided when the excluded volume of the chain segments is neglected.

We can analytically understand the nonuniform scaling by expanding the self-consistent closure Eq. **18** by assuming there is a power law but with adjusted exponents. If we have a pure power law decay $\mathscr{C}(x) \propto |x|^{-\nu}$, one finds that $\int_0^{\Delta s} dx \mathscr{C}(x)(\Delta s - x) = |\Delta s|^{2-\nu} \int_0^1 dx x^{-\nu}(1-x)$ scales also with a power of the genomic separation. From Eq. **17**, we have that $\langle r_{ss'}^2 \rangle = b_G^2|\Delta s|[1 - (\vartheta - \frac{1}{2})\frac{\kappa l^2}{dD}\mathcal{C}_T] + b_G^2(\vartheta - \frac{1}{2})\frac{\kappa l^2}{dD} Z_1(\nu)|\Delta s|^{2-\nu}$ for small Δs, where $Z_1(\nu)$ is a normalization constant (*SI Appendix*). The polymer chain is still Rouse-like at large scales, while it becomes crumpled at small scales with $\langle R_{ss'}^2 \rangle \propto |\Delta s|^{2-\nu}$. For self-consistency, the scaling exponent ν from Eq. **18** must then satisfy $\frac{3}{2}(\nu - 2) = -\nu$. This equality gives a self-consistent value of the scaling exponent $\nu = 1.2$, which agrees with the results of the numerical solutions. These predictions for the scaling behaviors are close to the experimental results of the interphase human chromosomes, where one finds $\gamma \approx 1.1$ (7). We estimate that the crossover to the nonuniform scalings happens at $\sim 10^4$ to 10^5 bp (*SI Appendix*), which also agrees with the experimental crossover seen for the human and Drosophila interphase chromosome which occurs at $\sim 10^5$ bp [$P_c(\Delta s) \sim \Delta s^{-1.1}$] (7, 103, 104).

Discussion. We have so far not explicitly concerned ourselves with "cohesin processivity." Cohesin processivity is determined by the residence time of the SMC head at the anchor points (105–107), relative to the time of making displacements. In the approximation studied here, the two quantities appear only as a composite in Q. Experiments have shown that when the wings-apart-like protein homolog is depleted, cohesins are unable to dissociate from chromatin, resulting in a greatly increased residence time τ_{re}, and prolonging the duration of loop extrusion (108, 109). In the weakly processive case, in contrast, the loading and detachment rates of the cohesins are both much greater than the compaction rate of the chromosome. The cohesin unbinds soon after a grappling displacement, indicative of short residence time. All sites on the polymer chain act as anchor points in an ergodic and equiprobable manner. This limit should be well captured by the self-consistent approximation since the extrusion probability can be replaced by a uniform distribution proportional to the average cohesin occupancy $\mathcal{T}$, which is only a function of genomic distance Δs, independent of the specific binding occupancy of cohesins. The weak processivity scenario resembles the transient-link-and-pass activity model (110, 111). In this model, enzymes lead to transient attractive connections between segments, and the timescale of enzyme unbinding is much shorter than the timescale of the chromatin dynamics. Additionally, the weak processivity assumption used in the formulation of a Markovian Master equation is similar to recently proposed diffusion encounter models (112, 113). These emphasize the transient bridging of the diffusively approaching chromatin segments by SMC proteins. These models are supported by recent biochemical data but conflict with the most popular loop extrusion model with high processivity. The two views have recently been contrasted (114, 115). If the grappling motor is highly processive, the effective kicking distance l and the grappling distance may also differ, and the present treatment may still be approximately valid, if the grappling capture lengths and step size are individually renormalized to account for multiple correlated steps. The residence time and binding rate of cohesin can vary over a wide range of parameter space values (116–118). In the highly processive scenario, the anchor point can be thought of as being "pinned" so that the next grappling event is more likely to occur locally rather than being spatially independent. This implies history dependence (16), which needs a non-Markovian treatment. We believe processivity becomes more significant for mitotic chromosomes, but we must leave the description of strongly correlated segment motions for future work.

Conclusion

Energy landscape theory has provided a powerful statistical mechanical tool for the quantitative study of complex nonequilibrium systems like chromosomes. The "ideal chromosome" model introduced by Zhang and Wolynes builds the local structure under motorization in a sequence translationally invariant potential form but is agnostic as to its origin (13, 14, 16). We have explored here how two classes of motors modify chromosome structure, one of which simply induces local reorganization while another class mimics grappling-induced loop extrusion. We show grappling motors can provide a mechanism for inducing the spatial correlation of the ideal chromosome as inferred from Hi-C experiments. Certainly, the models proposed here are not meant to be the final answers. Due to the excluded volume effect, chromosomes can become entangled with possible knotting, leading to widespread topological constraints. Although topoisomerases in cells may mitigate such effects (119), excluded volume cannot be ignored especially in the formation of mitotic chromosomes where liquid crystal-like orientational ordering occurs (13, 14, 120, 121). Additionally, while our model captures some topological changes such as the formation of loops, these are on a smaller scale than compartmentalization.

We have focused here on uniform motorizations of a homogeneous chain. Further investigation into heterogeneous polymer chain models will facilitate a deeper understanding of chromosomal compartmentalization phenomena (7, 122–124). We have also looked only at the time-averaged structural properties. Equally intriguing is the exploration of motorization's impact on the chromosome's coherent motion (20, 125–127) and how

chromosomal structures move and rearrange within the nucleus during the cell cycle and in response to cellular signaling (128).

Materials and Methods

Simulations. We carried out hybrid Brownian-Gillespie simulations of the polymer dynamics for the swimming motors: https://github.com/CaOaC/chromosome. The programs can run in parallel on Cuda software. We use periodic boundary conditions without considering the self-avoiding and excluded-volume effect. The parameters chosen are $\kappa l^2/dD = 1$ and $b^2 = 2$. We simulate for sufficiently long until the contact maps reach stable. Our database includes sample trajectories of 200 beads that can be viewed in open visualization tool (OVITO) (129). In addition, we solve the self-consistent equation Eq. **18** by an iterative method: https://github.com/CaOaC/chromosome. We set the initial ansatz to be $C(\Delta s) \sim \Delta s^{-1/2}$ without loss of generality and choose the fixed cutoff contact radius $a_0/2l = 0.1$.

Data, Materials, and Software Availability. Codes and example output files are available at https://github.com/CaOaC/chromosome (130). All other data are included in the manuscript and/or *SI Appendix*.

ACKNOWLEDGMENTS. We would like to thank Vinicius G. Contessoto and Sumitabha Brahmachari for their helpful discussions. P.G.W. was supported both by the Bullard–Welch Chair at Rice University, grant C-0016, and by the Center for Theoretical Biological Physics sponsored by NSF grant PHY-2019745.

1. J. E. Phillips, V. G. Corces, CTCF: Master weaver of the genome. *Cell* **137**, 1194–1211 (2009).
2. S. S. Rao *et al.*, A 3D map of the human genome at kilobase resolution reveals principles of chromatin looping. *Cell* **159**, 1665–1680 (2014).
3. B. Van Steensel, Chromatin: Constructing the big picture. *EMBO J.* **30**, 1885–1895 (2011).
4. R. Collepardo-Guevara *et al.*, Chromatin unfolding by epigenetic modifications explained by dramatic impairment of internucleosome interactions: A multiscale computational study. *J. Am. Chem. Soc.* **137**, 10205–10215 (2015).
5. T. Cremer, C. Cremer, Chromosome territories, nuclear architecture and gene regulation in mammalian cells. *Nat. Rev. Genet.* **2**, 292–301 (2001).
6. W. A. Bickmore, The spatial organization of the human genome. *Annu. Rev. Genomics Hum. Genet.* **14**, 67–84 (2013).
7. E. Lieberman-Aiden *et al.*, Comprehensive mapping of long-range interactions reveals folding principles of the human genome. *Science* **326**, 289–293 (2009).
8. K. E. Cullen, M. P. Kladde, M. A. Seyfred, Interaction between transcription regulatory regions of prolactin chromatin. *Science* **261**, 203–206 (1993).
9. J. Dekker, K. Rippe, M. Dekker, N. Kleckner, Capturing chromosome conformation. *Science* **295**, 1306–1311 (2002).
10. J. Dostie *et al.*, Chromosome conformation capture carbon copy (5C): A massively parallel solution for mapping interactions between genomic elements. *Genome Res.* **16**, 1299–1309 (2006).
11. Y. Qi, B. Zhang, Predicting three-dimensional genome organization with chromatin states. *PLoS Comput. Biol.* **15**, e1007024 (2019).
12. J. J. Messelink, M. C. van Teeseling, J. Janssen, M. Thanbichler, C. P. Broedersz, Learning the distribution of single-cell chromosome conformations in bacteria reveals emergent order across genomic scales. *Nat. Commun.* **12**, 1963 (2021).
13. B. Zhang, P. G. Wolynes, Topology, structures, and energy landscapes of human chromosomes. *Proc. Natl. Acad. Sci. U.S.A.* **112**, 6062–6067 (2015).
14. B. Zhang, P. G. Wolynes, Shape transitions and chiral symmetry breaking in the energy landscape of the mitotic chromosome. *Phys. Rev. Lett.* **116**, 248101 (2016).
15. M. Di Pierro, B. Zhang, E. L. Aiden, P. G. Wolynes, J. N. Onuchic, Transferable model for chromosome architecture. *Proc. Natl. Acad. Sci. U.S.A.* **113**, 12168–12173 (2016).
16. B. Zhang, P. G. Wolynes, Genomic energy landscapes. *Biophys. J.* **112**, 427–433 (2017).
17. M. Di Pierro, R. R. Cheng, E. Lieberman Aiden, P. G. Wolynes, J. N. Onuchic, De novo prediction of human chromosome structures: Epigenetic marking patterns encode genome architecture. *Proc. Natl. Acad. Sci. U.S.A.* **114**, 12126–12131 (2017).
18. M. Di Pierro, D. A. Potoyan, P. G. Wolynes, J. N. Onuchic, Anomalous diffusion, spatial coherence, and viscoelasticity from the energy landscape of human chromosomes. *Proc. Natl. Acad. Sci. U.S.A.* **115**, 7753–7758 (2018).
19. G. Shi, D. Thirumalai, From HI-C contact map to three-dimensional organization of interphase human chromosomes. *Phys. Rev. X* **11**, 011051 (2021).
20. A. Zidovska, D. A. Weitz, T. J. Mitchison, Micron-scale coherence in interphase chromatin dynamics. *Proc. Natl. Acad. Sci. U.S.A.* **110**, 15555–15560 (2013).
21. G. J. Narlikar, R. Sundaramoorthy, T. Owen-Hughes, Mechanisms and functions of ATP-dependent chromatin-remodeling enzymes. *Cell* **154**, 490–503 (2013).
22. F. Uhlmann, SMC complexes: From DNA to chromosomes. *Nat. Rev. Mol. Cell Biol.* **17**, 399–412 (2016).
23. M. A. Reid, Z. Dai, J. W. Locasale, The impact of cellular metabolism on chromatin dynamics and epigenetics. *Nat. Cell Biol.* **19**, 1298–1306 (2017).
24. D. Zwicker, The intertwined physics of active chemical reactions and phase separation. *Curr. Opin. Colloid Interface Sci.*, 101606 (2022).
25. D. Needleman, Z. Dogic, Active matter at the interface between materials science and cell biology. *Nat. Rev. Mater.* **2**, 1–14 (2017).
26. B. van Steensel, E. E. Furlong, The role of transcription in shaping the spatial organization of the genome. *Nat. Rev. Mol. Cell Biol.* **20**, 327–337 (2019).
27. K. Struhl, E. Segal, Determinants of nucleosome positioning. *Nat. Struct. Mol. Biol.* **20**, 267–273 (2013).
28. G. Fudenberg *et al.*, Formation of chromosomal domains by loop extrusion. *Cell Rep.* **15**, 2038–2049 (2016).
29. T. Shen, P. G. Wolynes, Stability and dynamics of crystals and glasses of motorized particles. *Proc. Natl. Acad. Sci. U.S.A.* **101**, 8547–8550 (2004).
30. T. Shen, P. G. Wolynes, Nonequilibrium statistical mechanical models for cytoskeletal assembly: Towards understanding tensegrity in cells. *Phys. Rev. E* **72**, 041927 (2005).
31. S. Wang, P. G. Wolynes, Communication: Effective temperature and glassy dynamics of active matter. *J. Chem. Phys.* **135**, 051101 (2011).
32. S. Wang, P. G. Wolynes, Tensegrity and motor-driven effective interactions in a model cytoskeleton. *J. Chem. Phys.* **136**, 145102 (2012).
33. S. C. Weber, A. J. Spakowitz, J. A. Theriot, Nonthermal ATP-dependent fluctuations contribute to the in vivo motion of chromosomal loci. *Proc. Natl. Acad. Sci. U.S.A.* **109**, 7338–7343 (2012).
34. N. Ganai, S. Sengupta, G. I. Menon, Chromosome positioning from activity-based segregation. *Nucleic Acids Res.* **42**, 4145–4159 (2014).
35. A. Agrawal, N. Ganai, S. Sengupta, G. I. Menon, Nonequilibrium biophysical processes influence the large-scale architecture of the cell nucleus. *Biophys. J.* **118**, 2229–2244 (2020).
36. Z. Jiang, Y. Qi, K. Kamat, B. Zhang, Phase separation and correlated motions in motorized genome. *J. Phys. Chem. B* **126**, 5619–5628 (2022).
37. A. Ghosh, A. J. Spakowitz, Active and thermal fluctuations in multi-scale polymer structure and dynamics. *Soft Matter* **18**, 6629–6637 (2022).
38. A. Goychuk, D. Kannan, A. K. Chakraborty, M. Kardar, Polymer folding through active processes recreates features of genome organization. *Proc. Natl. Acad. Sci. U.S.A.* **120**, e2221726120 (2023).
39. S. Brahmachari, T. Markovich, F. C. MacKintosh, J. N. Onuchic, Temporally correlated active forces drive chromosome structure and dynamics. bioRxiv [Preprint] (2023). https://doi.org/10.1101/2023.04.23.528410 (Accessed 24 August 2023).
40. A. Goychuk, D. Kannan, M. Kardar, Delayed excitations induce polymer looping and coherent motion. arXiv [Preprint] (2024). http://arxiv.org/abs/2401.14870 (Accessed 27 January 2024).
41. M. Ganji *et al.*, Real-time imaging of DNA loop extrusion by condensin. *Science* **360**, 102–105 (2018).
42. B. W. Bauer *et al.*, Cohesin mediates DNA loop extrusion by a "swing and clamp" mechanism. *Cell* **184**, 5448–5464 (2021).
43. R. Oldenkamp, B. D. Rowland, A walk through the SMC cycle: From catching DNAs to shaping the genome. *Mol. Cell* **82**, 1616–1630 (2022).
44. C. Dekker, C. H. Haering, J. M. Peters, B. D. Rowland, How do molecular motors fold the genome? *Science* **382**, 646–648 (2023).
45. I. A. Shaltiel *et al.*, A hold-and-feed mechanism drives directional DNA loop extrusion by condensin. *Science* **376**, 1087–1094 (2022).
46. S. Wang, P. G. Wolynes, On the spontaneous collective motion of active matter. *Proc. Natl. Acad. Sci. U.S.A.* **108**, 15184–15189 (2011).
47. S. Wang, P. G. Wolynes, Active contractility in actomyosin networks. *Proc. Natl. Acad. Sci. U.S.A.* **109**, 6446–6451 (2012).
48. M. Dogterom, B. Yurke, Measurement of the force-velocity relation for growing microtubules. *Science* **278**, 856–860 (1997).
49. J. Howard, R. Clark, Mechanics of motor proteins and the cytoskeleton. *Appl. Mech. Rev.* **55**, B39–B39 (2002).
50. S. Wang, P. G. Wolynes, Active patterning and asymmetric transport in a model actomyosin network. *J. Chem. Phys.* **139**, 235103 (2013).
51. A. B. Kolomeisky, *Motor Proteins and Molecular Motors* (CRC Press, 2015).
52. X. Bai, P. G. Wolynes, On the hydrodynamics of swimming enzymes. *J. Chem. Phys.* **143**, 165101 (2015).
53. A. B. Kolomeisky, M. E. Fisher, Molecular motors: A theorist's perspective. *Annu. Rev. Phys. Chem.* **58**, 675–695 (2007).
54. L. Zhang, D. A. Silva, F. Pardo-Avila, D. Wang, X. Huang, Structural model of RNA polymerase ii elongation complex with complete transcription bubble reveals NTP entry routes. *PLoS Comput. Biol.* **11**, e1004354 (2015).
55. K. A. Hagstrom, B. J. Meyer, Condensin and cohesin: More than chromosome compactor and glue. *Nat. Rev. Genet.* **4**, 520–534 (2003).
56. S. Yatskevich, J. Rhodes, K. Nasmyth, Organization of chromosomal DNA by SMC complexes. *Annu. Rev. Genet.* **53**, 445–482 (2019).
57. J. M. Eeftens *et al.*, Condensin SMC2–SMC4 dimers are flexible and dynamic. *Cell Rep.* **14**, 1813–1818 (2016).
58. I. Kulemzina *et al.*, A reversible association between SMC coiled coils is regulated by lysine acetylation and is required for cohesin association with the DNA. *Mol. Cell* **63**, 1044–1054 (2016).
59. M. T. Hons *et al.*, Topology and structure of an engineered human cohesin complex bound to Pds5B. *Nat. Commun.* **7**, 12523 (2016).
60. F. Bürmann *et al.*, Tuned SMC arms drive chromosomal loading of prokaryotic condensin. *Mol. Cell* **65**, 861–872 (2017).
61. D. Krepel, R. R. Cheng, M. Di Pierro, J. N. Onuchic, Deciphering the structure of the condensin protein complex. *Proc. Natl. Acad. Sci. U.S.A.* **115**, 11911–11916 (2018).
62. M. Yamauchi, G. B. Brandani, T. Terakawa, S. Takada, SMC complex unidirectionally translocates DNA by coupling segment capture with an asymmetric kleisin path. bioRxiv [Preprint] (2024). https://doi.org/10.1101/2024.04.29.591782 (Accessed 3 May 2024).
63. D. Krepel, A. Davtyan, N. P. Schafer, P. G. Wolynes, J. N. Onuchic, Braiding topology and the energy landscape of chromosome organization proteins. *Proc. Natl. Acad. Sci. U.S.A.* **117**, 1468–1477 (2020).

64. Z. Jiang, B. Zhang, Theory of active chromatin remodeling. *Phys. Rev. Lett.* **123**, 208102 (2019).
65. B. H. Zimm, Dynamics of polymer molecules in dilute solution: Viscoelasticity, flow birefringence and dielectric loss. *J. Chem. Phys.* **24**, 269–278 (1956).
66. M. Doi, S. F. Edwards, S. F. Edwards, *The Theory of Polymer Dynamics* (Oxford University Press, 1988), vol. 73.
67. P. G. De Gennes, Quasi-elastic scattering of neutrons by dilute polymer solutions: I. Free-draining limit. *Phys. Phys. Fiz.* **3**, 37 (1967).
68. M. Fixman, Highly anharmonic crystal. *J. Chem. Phys.* **51**, 3270–3279 (1969).
69. J. Stoessel, P. Wolynes, Linear excitations and the stability of the hard sphere glass. *J. Chem. Phys.* **80**, 4502–4512 (1984).
70. Y. Singh, J. Stoessel, P. Wolynes, Hard-sphere glass and the density-functional theory of aperiodic crystals. *Phys. Rev. Lett.* **54**, 1059 (1985).
71. M. Mézard, G. Parisi, Thermodynamics of glasses: A first principles computation. *J. Phys. Condens. Matter* **11**, A157 (1999).
72. R. W. Hall, P. G. Wolynes, Microscopic theory of network glasses. *Phys. Rev. Lett.* **90**, 085505 (2003).
73. T. Jenuwein, C. D. Allis, Translating the histone code. *Science* **293**, 1074–1080 (2001).
74. R. Margueron, D. Reinberg, Chromatin structure and the inheritance of epigenetic information. *Nat. Rev. Genet.* **11**, 285–296 (2010).
75. C. Bechinger *et al*., Active particles in complex and crowded environments. *Rev. Mod. Phys.* **88**, 045006 (2016).
76. S. Shin, H. W. Cho, G. Shi, D. Thirumalai, Transcription-induced active forces suppress chromatin motion by inducing a transient disorder-to-order transition. *Biophys. J.* **122**, 19a (2023).
77. S. F. Edwards, The statistical mechanics of polymers with excluded volume. *Proc. Phys. Soc.* **85**, 613 (1965).
78. M. Muthukumar, S. Edwards, Extrapolation formulas for polymer solution properties. *J. Chem. Phys.* **76**, 2720–2730 (1982).
79. M. Muthukumar, Brownian dynamics of polymer chains in membranes. *J. Chem. Phys.* **82**, 5696–5706 (1985).
80. M. Muthukumar, Adsorption of a polyelectrolyte chain to a charged surface. *J. Chem. Phys.* **86**, 7230–7235 (1987).
81. W. Schwarzer *et al*., Two independent modes of chromatin organization revealed by cohesin removal. *Nature* **551**, 51–56 (2017).
82. C. Vara *et al*., Three-dimensional genomic structure and cohesin occupancy correlate with transcriptional activity during spermatogenesis. *Cell Rep.* **28**, 352–367 (2019).
83. K. Nasmyth, C. H. Haering, Cohesin: Its roles and mechanisms. *Annu. Rev. Genet.* **43**, 525–558 (2009).
84. S. Edwards, The size of a polymer molecule in a strong solution. *J. Phys. A Math. Gen.* **8**, 1670 (1975).
85. S. F. Edwards, P. Singh, Size of a polymer molecule in solution. Part 1.–Excluded volume problem. *J. Chem. Soc. Faraday Trans. 2 Mol. Chem. Phys.* **75**, 1001–1019 (1979).
86. L. Mirny, J. Dekker, Mechanisms of chromosome folding and nuclear organization: Their interplay and open questions. *Cold Spring Harb. Perspect. Biol.* **14**, a040147 (2022).
87. A. Grosberg, Y. Rabin, S. Havlin, A. Neer, Crumpled globule model of the three-dimensional structure of DNA. *Europhys. Lett.* **23**, 373 (1993).
88. A. Y. Grosberg, S. K. Nechaev, E. I. Shakhnovich, The role of topological constraints in the kinetics of collapse of macromolecules. *J. Phys.* **49**, 2095–2100 (1988).
89. J. D. Halverson, J. Smrek, K. Kremer, A. Y. Grosberg, From a melt of rings to chromosome territories: The role of topological constraints in genome folding. *Rep. Prog. Phys.* **77**, 022601 (2014).
90. L. A. Mirny, The fractal globule as a model of chromatin architecture in the cell. *Chromosome Res.* **19**, 37–51 (2011).
91. A. Y. Grosberg, Annealed lattice animal model and flory theory for the melt of non-concatenated rings: Towards the physics of crumpling. *Soft Matter* **10**, 560–565 (2014).
92. A. Rosa, R. Everaers, Ring polymers in the melt state: The physics of crumpling. *Phys. Rev. Lett.* **112**, 118302 (2014).
93. K. Polovnikov, S. Nechaev, M. Tamm, Effective hamiltonian of topologically stabilized polymer states. *Soft matter* **14**, 6561–6570 (2018).
94. K. Polovnikov, M. Gherardi, M. Cosentino-Lagomarsino, M. Tamm, Fractal folding and medium viscoelasticity contribute jointly to chromosome dynamics. *Phys. Rev. Lett.* **120**, 088101 (2018).
95. K. E. Polovnikov *et al*., Crumpled polymer with loops recapitulates key features of chromosome organization. *Phys. Rev. X* **13**, 041029 (2023).
96. S. S. Rao *et al*., Cohesin loss eliminates all loop domains. *Cell* **171**, 305–320 (2017).
97. T. H. S. Hsieh *et al*., Enhancer-promoter interactions and transcription are largely maintained upon acute loss of CTCF, cohesin, WAPL or YY1. *Nat. Genet.* **54**, 1919–1932 (2022).
98. K. Polovnikov, B. Slavov, Topological and nontopological mechanisms of loop formation in chromosomes: Effects on the contact probability. *Phys. Rev. E* **107**, 054135 (2023).
99. L. I. Nazarov, M. V. Tamm, V. A. Avetisov, S. K. Nechaev, A statistical model of intra-chromosome contact maps. *Soft matter* **11**, 1019–1025 (2015).
100. M. Marsden, U. Laemmli, Metaphase chromosome structure: Evidence for a radial loop model. *Cell* **17**, 849–858 (1979).
101. A. L. Sanborn *et al*., Chromatin extrusion explains key features of loop and domain formation in wild-type and engineered genomes. *Proc. Natl. Acad. Sci. U.S.A.* **112**, E6456–E6465 (2015).
102. S. Brahmachari, J. F. Marko, Chromosome disentanglement driven via optimal compaction of loop-extruded brush structures. *Proc. Natl. Acad. Sci. U.S.A.* **116**, 24956–24965 (2019).
103. S. K. Ghosh, D. Jost, How epigenome drives chromatin folding and dynamics, insights from efficient coarse-grained models of chromosomes. *PLoS Comput. Biol.* **14**, e1006159 (2018).
104. T. Sexton *et al*., Three-dimensional folding and functional organization principles of the Drosophila genome. *Cell* **148**, 458–472 (2012).
105. E. Alipour, J. F. Marko, Self-organization of domain structures by DNA-loop-extruding enzymes. *Nucleic Acids Res.* **40**, 11202–11212 (2012).
106. A. Goloborodko, J. F. Marko, L. A. Mirny, Chromosome compaction by active loop extrusion. *Biophys. J.* **110**, 2162–2168 (2016).
107. B. Chan, M. Rubinstein, Theory of chromatin organization maintained by active loop extrusion. *Proc. Natl. Acad. Sci. U.S.A.* **120**, e2222078120 (2023).
108. S. Kueng *et al*., WAPL controls the dynamic association of cohesin with chromatin. *Cell* **127**, 955–967 (2006).
109. A. Tedeschi *et al*., WAPL is an essential regulator of chromatin structure and chromosome segregation. *Nature* **501**, 564–568 (2013).
110. R. Das, T. Sakaue, G. Shivashankar, J. Prost, T. Hiraiwa, How enzymatic activity is involved in chromatin organization. *eLife* **11**, e79901 (2022).
111. R. Das, T. Sakaue, G. Shivashankar, J. Prost, T. Hiraiwa, Chromatin remodeling due to transient-link-and-pass activity enhances subnuclear dynamics. *Phys. Rev. Lett.* **132**, 058401 (2024).
112. M. Tang *et al*., Establishment of dsDNA-dsDNA interactions by the condensin complex. *Mol. Cell* **83**, 3787–3800 (2023).
113. T. M. Guerin, C. Barrington, G. Pobegalov, M. I. Molodtsov, F. Uhlmann, Cohesin chromatin loop formation by an extrinsic motor. bioRxiv [Preprint] (2023). https://doi.org/10.1101/2023.11.30.569410 (Accessed 11 May 2024).
114. T. Nozaki *et al*., Condensed but liquid-like domain organization of active chromatin regions in living human cells. *Sci. Adv.* **9**, eadf1488 (2023).
115. L. Lizana, Y. B. Schwartz, The scales, mechanisms, and dynamics of the genome architecture. *Sci. Adv.* **10**, eadm8167 (2024).
116. J. H. Gibcus *et al*., A pathway for mitotic chromosome formation. *Science* **359**, eaao6135 (2018).
117. P. Mach *et al*., Cohesin and CTCF control the dynamics of chromosome folding. *Nat. Genet.* **54**, 1907–1918 (2022).
118. L. Costantino, T. H. S. Hsieh, R. Lamothe, X. Darzacq, D. Koshland, Cohesin residency determines chromatin loop patterns. *eLife* **9**, e59889 (2020).
119. J. R. Swedlow, J. W. Sedat, D. A. Agard, Multiple chromosomal populations of topoisomerase II detected in vivo by time-lapse, three-dimensional wide-field microscopy. *Cell* **73**, 97–108 (1993).
120. N. Naumova *et al*., Organization of the mitotic chromosome. *Science* **342**, 948–953 (2013).
121. E. B. De La Tour, U. Laemmli, The metaphase scaffold is helically folded: Sister chromatids have predominantly opposite helical handedness. *Cell* **55**, 937–944 (1988).
122. T. Misteli, The self-organizing genome: Principles of genome architecture and function. *Cell* **183**, 28–45 (2020).
123. I. Solovei, K. Thanisch, Y. Feodorova, How to rule the nucleus: Divide et impera. *Curr. Opin. Cell Biol.* **40**, 47–59 (2016).
124. M. Falk *et al*., Heterochromatin drives compartmentalization of inverted and conventional nuclei. *Nature* **570**, 395–399 (2019).
125. T. J. Lampo, A. S. Kennard, A. J. Spakowitz, Physical modeling of dynamic coupling between chromosomal loci. *Biophys. J.* **110**, 338–347 (2016).
126. D. Saintillan, M. J. Shelley, A. Zidovska, Extensile motor activity drives coherent motions in a model of interphase chromatin. *Proc. Natl. Acad. Sci. U.S.A.* **115**, 11442–11447 (2018).
127. I. Eshghi, A. Zidovska, A. Y. Grosberg, Activity-driven phase transition causes coherent flows of chromatin. *Phys. Rev. Lett.* **131**, 048401 (2023).
128. T. T. Su, Cellular responses to DNA damage: One signal, multiple choices. *Annu. Rev. Genet.* **40**, 187–208 (2006).
129. A. Stukowski, Visualization and analysis of atomistic simulation data with OVITO-the open visualization tool. *Modell. Simul. Mater. Sci. Eng.* **18**, 015012 (2009).
130. Z. Cao, P. G. Wolynes, Source Code–Motorized chain models of the ideal chromosome. Zenodo. http://doi.org/10.5281/zenodo.12193234. Deposited 20 June 2024.